



OPEN Mechanical properties and microscopic features of LBM-GGBS solidified saline soil in seasonally frozen areas

Shanyan Chen^{1,2}, Pengfei Ren^{1,2}✉, Junyi Wang³✉, Ming-Zhi Guo^{1,2}, Yang Zhao^{1,2}, Ziqing He¹, Gang Hou¹ & Jiang-Shan Li⁴

Light-Burned Magnesia (LBM) activated Ground Granulated Blast Furnace Slag (GGBS) is established as a promising and robust binder for soil stabilization. However, its durability in saline environments subjected to freeze-thaw (F-T) cycles lacks systematic investigation. To validate its potential for subgrade engineering in seasonally frozen regions, this study evaluates the mechanical and microscopic properties of LBM-GGBS solidified saline soil under F-T cycling. The effects of LBM and GGBS on the unconfined compressive strength (UCS), permeability coefficient, Cl⁻ leaching and microstructures of solidified saline soil after different F-T cycles (0, 2, 4, 6, 8, and 10) were examined. The results showed that increasing the LBM-GGBS content significantly enhanced the soil's resistance to F-T cycles. With a 12% LBM-GGBS content and a GGBS/LBM ratio of 7 (determined as the optimal mix proportion), the solidified soil reached a residual strength of 3 MPa after 10 F-T cycles, which was four times the strength required for the upper base layer of highway pavement subgrade. Microscopic analysis revealed that the LBM-GGBS solidified soil exhibited a dense structure with calcium silicate hydrate (C-S-H), magnesium silicate hydrate (M-S-H), hydrotalcite, and Kuzel salt as the primary reaction products. The formation of these hydration products significantly densified the structure, thereby increasing the strength and improving the F-T resistance of the solidified soil. Furthermore, ~75% of Cl⁻ in the original saline soil could be stabilized even after multiple F-T cycles. These findings elucidate the micro-mechanism of chloride stabilization under freezing conditions and provide a robust theoretical foundation for utilizing LBM-GGBS to mitigate saline soil hazards in seasonally frozen regions.

Keywords Chloride saline soil, Ground granulated blast furnace slag, Light-burned magnesia, Freeze-thaw cycles, Microstructure

Saline soil is defined by a soluble salt content exceeding 0.3%¹. More than 833 million hectares of saline soil have formed globally as a result of both human activities and natural processes². The presence of substantial amounts of soluble and insoluble salts in saline soil results in complex interactions between solid and liquid phases under fluctuating environmental conditions such as temperature, humidity, and air pressure³. This complexity presents challenges for the effective utilization of saline soil. In northwestern China, various types of saline soil are prevalent in regions that experience seasonal freezing^{4,5}. This area undergoes a freeze-thaw (F-T) cycle lasting approximately five months each year, with the possibility of daily F-T cycles under extreme weather conditions. Such harsh environmental conditions significantly affect the soil's structure and mechanical properties. Using saline soil directly as subgrade material in this region can lead to engineering issues such as mud pumping, dissolution, subsidence, and uneven settlement^{6,7}. These engineering and geological challenges severely limit subgrade construction in the area. Thus, there is an urgent need to develop effective saline soil treatment technologies to enable its use as a road-filling material.

¹School of Civil Engineering, Shaoxing University, Shaoxing, Zhejiang, China. ²Institute for Advanced Study, Shaoxing University, Shaoxing, Zhejiang, China. ³China Construction Eighth Engineering Division (Shandong) New Material Technology CO., LTD., Jinan 250020, China. ⁴State Key Laboratory of Geomechanics and Geotechnical Engineering Safety, Institute of Rock and Soil Mechanics, Chinese Academy of Sciences, Wuhan 430071, China. ✉email: renpf@usx.edu.cn; wangjy_cscec8ud@163.com

Water content (%)	Total salt content (%)	Natural density (g/cm ³)	Liquid limit (%)	Plastic limit (%)	Optimum water content (%)	Maximum dry density (g/cm ³)	Size distribution (%)		
							Sand	Silt	Clay
10.02	1.40	1.17	21.50	10.90	15.41	1.89	23.32	62.44	14.24

Table 1. Physical properties of saline soil. Water content is the field moisture of soil at the time of collection.

Ionic species	Cl ⁻	SO ₄ ²⁻	CO ₃ ²⁻	HCO ₃ ²⁻	Na ⁺	K ⁺	Mg ²⁺	Ca ²⁺
Content (mg/kg)	404.1	193.5	1260	388.8	4941	27.54	33.66	23.76

Table 2. Ion content of saline soil.

Stabilization/solidification (S/S) by incorporating Portland cement (PC) is a widely adopted and cost-effective method for improving the physical properties of saline soil^{8,9}. However, the production of PC has significant environmental drawbacks, including high CO₂ emissions and energy consumption¹⁰. Additionally, PC is susceptible to expansive damage when used to solidify saline soils, particularly those with a high salt content¹¹. Consequently, there is a growing interest in using industrial by-products as sustainable alternatives to PC for saline soil S/S. Ground granulated blast furnace slag (GGBS), a by-product of the iron industry, has emerged as a promising alternative¹². Typically activated with an alkali, GGBS has been successfully applied in soil treatment (more suitable than PC), especially in saline soils containing chlorides and sulfates¹³. It offers higher compressive strength, lower permeability, and superior resistance to F-T cycles. Yi et al.¹⁴ found that lime-activated GGBS used in marine soil stabilization resulted in reduced porosity and a 90-day unconfined compressive strength 1.7 times greater than that achieved with PC. Similarly, Liu et al.¹⁵ applied a lime-gypsum-GGBS stabilizer to saline soils and obtained excellent unconfined compressive strength and water stability after 28 and 90 days of curing, meeting the requirements for general engineering foundation stabilization.

In recent years, light-burned magnesia (LBM), also known as reactive magnesia (MgO), has emerged as a sustainable activator for GGBS, alongside the more commonly used Ca(OH)₂¹⁶. LBM is typically produced by calcining magnesia at temperatures between 700 and 1000 °C, resulting in low crystallinity, a large specific surface area, and high reactivity¹⁷. Compared with Ca(OH)₂, LBM has demonstrated a greater efficiency in activating GGBS, leading to enhanced strength development in stabilized soils¹⁸. Yi et al.¹⁹ found that 5–10% LBM-activated GGBS improved the 28-day soil strength by roughly 30% compared with Ca(OH)₂ activation, primarily due to the increased hydrotalcite formation and matrix densification. Furthermore, higher dosages (10–20%) of LBM-activated GGBS have been shown to produce a greater volume of hydration products, yielding strengths up to four times higher than those of the Ca(OH)₂-based systems²⁰. In China, where most saline soils are located in the seasonally frozen regions of the northwest, resistance to F-T cycles is crucial. Numerous studies have demonstrated that soils solidified with LBM and/or cementitious materials exhibit strong resistance to F-T damage. Wang et al.²¹ investigated the effect of F-T cycles on the Pb²⁺-contaminated soils stabilized with MgO and MgO-fly ash. Their findings showed that soils solidified with just 0.5% stabilizer retained over 75% of their strength after 11 F-T cycles, meeting specification requirements. Cai et al.²² explored the F-T durability of the LBM-carbonated soils and found that the strength and modulus of the LBM-carbonated silt were twice as high as those of the PC-stabilized specimens. However, the existing literature has predominantly focused on non-saline soils or contaminants other than soluble salts. Research concerning the durability of LBM-GGBS stabilized saline soil under the rigorous coupled effects of chemical erosion (high salinity) and physical deterioration (F-T cycles) remains remarkably scarce. Specifically, the stability of chloride-binding hydration products under cyclic freezing conditions is not yet fully understood, rendering the long-term performance of this system unpredictable in cold and arid regions.

To address this critical knowledge gap, this study investigated the use of various dosages and ratios of LBM and GGBS to solidify saline soils under simulated F-T conditions. The unconfined compressive strength, Cl⁻ leaching, and permeability of the LBM-GGBS solidified saline soil before and after F-T cycles were examined. Scanning electron microscopy (SEM), energy-dispersive X-ray spectroscopy (EDS), and mercury intrusion porosimetry (MIP) were employed to elucidate microstructural evolution and chloride stabilization mechanisms. The novel insights into the chemical and physical stability of the solidified matrix presented herein are expected to provide a theoretical foundation for the practical application of LBM-based materials in stabilizing saline soils during frozen seasons.

Materials and methods

Materials

The saline soil was collected from a depth of 20–40 cm in Yulin City, Shaanxi Province, a region characterized by a typical seasonally frozen arid climate with an average maximum frost depth of 99 cm. The physical properties of the soil, tested in accordance with the *Standard for Geotechnical Testing Method* (GB/T 50123 – 2019)²³, are summarized in Table 1. For chemical analysis, soluble ions were extracted using a soil-to-water mass ratio of 1:5. The suspension was agitated, centrifuged, and filtered through a 0.45 μm PES membrane before being analyzed via ion chromatography (Table 2). Based on the *Code for Investigation of Geotechnical Engineering* (GB 50021 – 2001)²⁴, the soil is classified as a medium-chloride saline soil. This classification is supported by a total soluble salt content of 1.4% (determined via the leachate evaporation method) and a c(Cl⁻)/2c(SO₄²⁻) ratio

Raw materials	Chemical composition (%)						
	CaO	SiO ₂	Fe ₂ O ₃	Al ₂ O ₃	MgO	K ₂ O	Na ₂ O
GGBS	45.07	29.36	0.37	13.07	8.16	0.37	0.48
LBM	/	/	/	/	>99.00	/	/
Saline soil	4.71	69.96	1.84	9.51	1.95	2.09	2.15

Table 3. Chemical compositions of raw materials.

Sample ID	LBM-GGBS content (%)	GGBS/LBM
CS14-7	14	7:1
CS14-6	14	6:1
CS14-5	14	5:1
CS14-4	14	4:1
CS12-7	12	7:1
CS12-6	12	6:1
CS12-5	12	5:1
CS12-4	12	4:1
CS10-7	10	7:1
CS10-6	10	6:1
CS10-5	10	5:1
CS10-4	10	4:1
CS8-7	8	7:1
CS8-6	8	6:1
CS8-5	8	5:1
CS8-4	8	4:1

Table 4. Mix proportions of solidified saline soil samples.

(calculated based on Table 2) of 2.85, which exceeds the threshold of 2.0. Ground granulated blast furnace slag (GGBS) was obtained from an iron plant in Wuhan, and Light-Burned Magnesia (LBM) was produced by China Metallurgical Xindu Alloy Co., Ltd., with a purity of $\geq 99\%$. The chemical compositions of GGBS, LBM, and saline soil were tested using an X-ray fluorescence spectrometer (XRF), as shown in Table 3.

Sample preparation

Prior to all experiments, the saline soil was oven-dried at 105 °C, then crushed and passed through a 2 mm sieve for use. To simulate the wet mixing conditions typically encountered in subgrade stabilization engineering, the treated saline soil was thoroughly mixed with GGBS and LBM for 2 min. A fixed liquid to solid ratio of 0.3 (approximately 1.4 times the liquid limit) was adopted to create a flowable paste, ensuring homogeneous mixing and uniform hydration while avoiding density variations from dynamic compaction. After thorough mixing, the slurry was cast into a $\Phi 50 \times 50$ mm plastic mold in three layers, with each layer subjected to 1 min of vibration to minimize variations in dry density and eliminate entrapped air. After curing for 1 day, the samples were demolded and sealed in a curing chamber under standard conditions (temperature 23 ± 2 °C, humidity $\geq 95\%$) for 27 days. Based on prior research findings^{25,26}, GGBS can be effectively activated at 10% MgO, and the optimal durability of the solidified soil was achieved at a binder dosage of 10–15%. Consequently, this experiment was designed with an LBM-GGBS to saline soil mass ratio ranging from 8 to 14% in 2% increments, and a GGBS to LBM mass ratio varying from 4:1 to 7:1, resulting in a total of 16 groups. The specific mix proportions are listed in Table 4. The samples were labeled based on the LBM-GGBS content and the mass ratio of GGBS to LBM. For instance, CS12-7 denotes chloride saline soil (CS) stabilized with a 12% binder dosage and a GGBS to LBM ratio of 7:1.

Testing methods

Freeze-thaw cycle

After 28-day curing, samples were wrapped in a plastic film and placed in sealed bags to maintain constant moisture during the test. The samples were then placed in a freezer at -20 °C for 24 h. After freezing, they were allowed to thaw at 25 °C for 24 h, which constituted one F-T cycle (denoted as N_{F-T} where $N_{F-T=n}$ represents n cycles of F-T). After reaching the specified number of cycles (2, 4, 6, 8, and 10 times), the unconfined compressive strength (UCS), Cl^- leaching, permeability coefficient, and microstructure of solidified soils were evaluated subsequently.

Unconfined compressive strength

The UCS test was conducted using a universal testing machine in accordance with the *Standard for Geotechnical Testing Method* (GB/T50123-2019)²³. The loading rate was set at 0.5 mm/min, and the UCS was denoted as q_u .

Permeability

The permeability test was conducted using the constant head method with a flexible wall permeameter, in accordance with ASTM D5084²⁷. Initially, the samples were vacuumed in a saturation device under a negative pressure of -100 kPa for 1 h to remove entrapped air. Water was then introduced into the saturator to immerse the specimens. After a 24-hour saturation period, the samples were promptly removed for the permeability test. The resulting saturation degree of solidified soil reached 96.4%, meeting the ASTM D5084 criterion ($\geq 95\%$) for saturated hydraulic conductivity testing. During the test, the confining pressure was maintained at 80 kPa, while the inlet water pressure was kept at 60 kPa. Distilled water served as the permeating medium, and the test was performed at a room temperature of 25 °C. Readings from the inlet pipe were recorded at regular intervals until the difference between the inlet and outlet pipe readings stabilized.

Microstructures and pore structures

Samples subjected to 0, 2, and 10 F-T cycles were selected for microstructural and pore structure analyses based on the macroscopic UCS evolution trends: 0 cycles served as the reference; 2 cycles represented the critical stage of a sharp strength loss; and 10 cycles corresponded to the stabilized residual strength stage. After removing the peeled surface layer, the central part of each sample was placed in a freezer at -50 °C. The samples were then dehydrated using a freeze dryer under vacuum conditions for 48 h. The freeze-dried samples were subsequently cut into blocks for analysis using scanning electron microscopy (SEM) and mercury intrusion porosimetry (MIP). The microstructures of the solidified soil were analyzed using the TESCAN MIRA LMS SEM at magnifications of 1000 \times and 5000 \times . Meanwhile, the pore structures of the solidified soil were examined with the AutoPore IV 9520 high-performance automatic mercury porosimeter from Micromeritics.

Cl⁻ leaching

The chloride (Cl⁻) leaching from the original saline soil and sample CS12-7 after 0, 2, and 10 F-T cycles was measured using an ion chromatograph. To prepare the suspension, 10 g of the dried saline soil before solidification and freeze-dried powder of the solidified soil (10 + 10 \times LBM-GGBS content) were mixed with distilled water at a solid-to-water ratio of 1:5. The suspension was then shaken at a speed of 110 strokes per minute on a horizontal shaker for 8 h and allowed to stand for 6 h. The supernatant was collected using a syringe and filtered through a 0.45 μ m PES membrane for testing.

Results and discussion

Effect of F-T cycles on UCS

Figure 1a–d illustrate the variation in UCS for samples with different amounts of GGBS and LBM after undergoing various F-T cycles. It is evident that the strength of the solidified soil increases with a higher LBM-GGBS content at a fixed GGBS to LBM ratio. For instance, at a GGBS/LBM ratio of 4, the 28-day UCS of solidified soil increases from 1.94 to 5.54 MPa with increasing the LBM-GGBS content from 8 to 14%. However, when the LBM-GGBS content increases from 12 to 14%, the strength gains are not significant for all the groups, and the strength of the CS14-7 group even decreases. At a given LBM-GGBS content, a higher GGBS/LBM ratio generally corresponds to a higher UCS. Nonetheless, when the GGBS/LBM ratio increases to 7, the strength of the CS10, CS12, and CS14 groups decreases to varying degrees. This decline is attributed to the excessive presence of GGBS, which leads to the accumulation of un-hydrated particles within the saline soil structure, thereby adversely affecting the strength of the solidified soil²⁸.

The results of the strength changes after the 0 to 10 F-T cycles indicate that the variation in UCS (q_u) for all samples follows a consistent pattern, with the most significant decrease occurring after the second F-T cycle. For instance, the q_u of CS12-6 decreases from 6.53 to 3.17 MPa after the first two cycles, representing a 57% loss. Although q_u fluctuates after the second cycle among different groups, it tends to stabilize, with variations within a range of 0.5 MPa. After 10 F-T cycles, the q_u for samples with an 8–14% LBM-GGBS content ranges from 1 to 2, 1.8–2.6, 2–3, and 3.8–4.8 MPa, respectively. It is clear that increasing the content of LBM-GGBS significantly enhances the UCS of the solidified soil after F-T cycles. In the CS8-5 group, the q_u decreases from 1.94 MPa to a minimum of 1.06 MPa after 10 F-T cycles, which still meets the UCS requirements for the upper base layer as specified in the *Highway Pavement Subgrade Construction Technical Specifications* (JTJ 034-2000)²⁹.

To more clearly illustrate the variation in UCS (q_u) after F-T cycles, the strength residual coefficient (q_n) is defined. This coefficient is the ratio of the strength after n F-T cycles (where $n = 2, 4, 6, 8, \text{ and } 10$) to the strength before any F-T cycles. A higher q_n corresponds to less damage to the sample after F-T cycles. Figure 2a and b show the variation of q_n for the 12% and 14% LBM-GGBS incorporated samples, respectively. It can be observed that after 2 F-T cycles, the change in q_n is not significant. For series CS12, q_n ranges from 0.3 to 0.5 as GGBS/LBM increases from 4 to 7; for series CS14, it ranges from 0.55 to 0.8. This indicates that a higher GGBS/LBM ratio enhances the resistance to F-T damage. Figures 1c and 2b demonstrate that after 10 F-T cycles, the residual strength of CS12-7 still reaches 3 MPa, which is four times that of the UCS requirement for the upper base layer specified in the “Highway Pavement Subgrade Construction Technical Specifications” (JTJ 034-2000)²⁹. Compared with LBM, GGBS is more cost-effective. Thus, considering both the strength and economic factors, CS12-7 was determined to be the optimal mix proportion and was selected for the subsequent microstructural testing and analysis.

Figure 3 presents the stress-strain curves of series CS12 after 0 and 2 F-T cycles. Before undergoing F-T cycles, all samples display stress-strain curves typical of strain softening, with the failure strain stabilizing

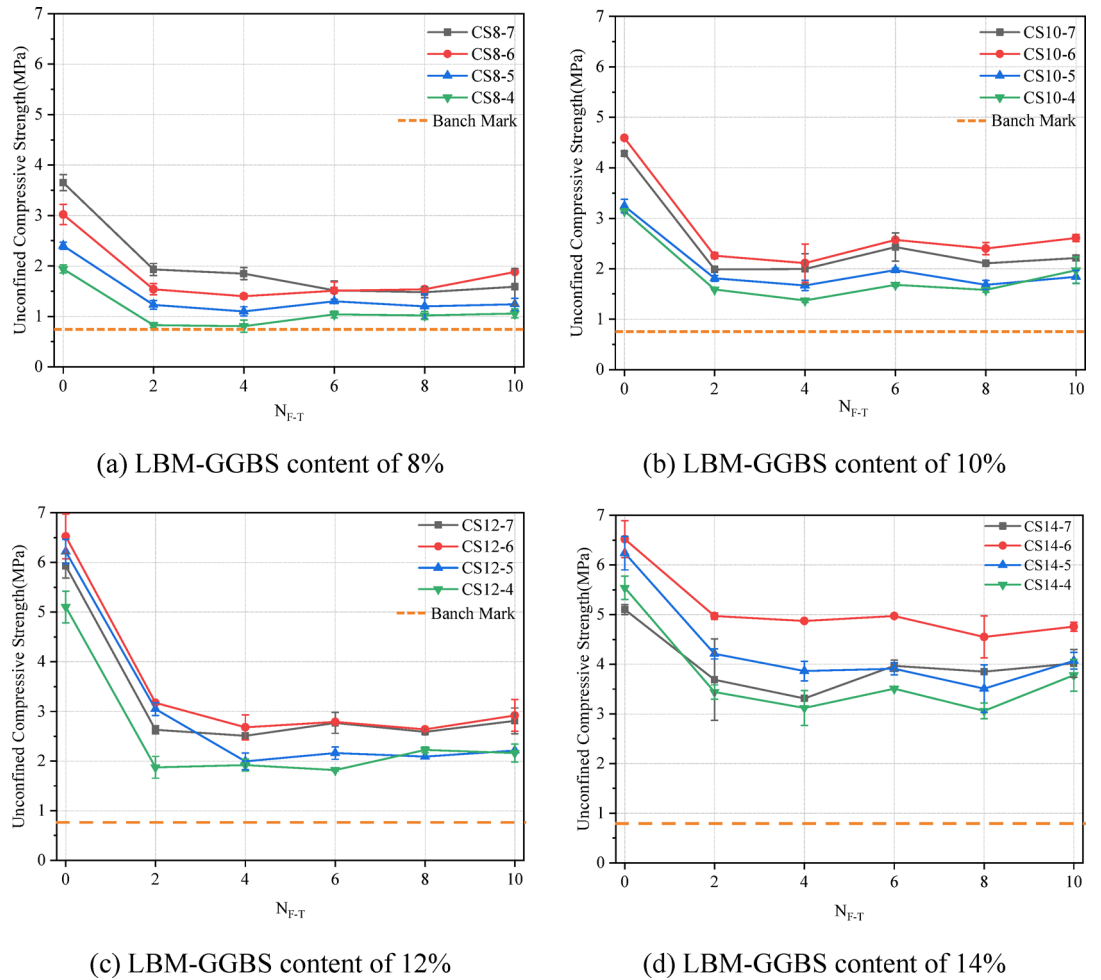


Fig. 1. UCS of solidified saline soil after F-T cycles.

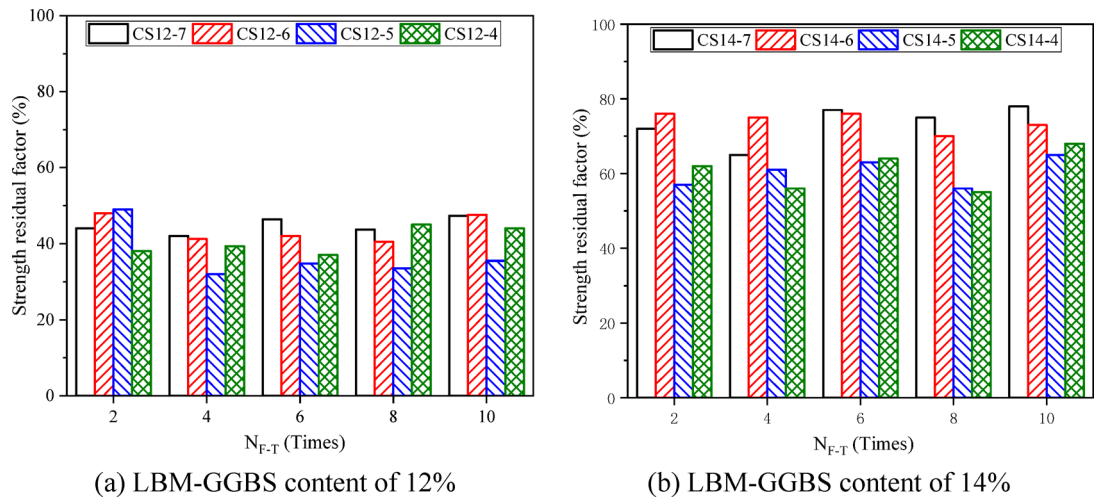


Fig. 2. Residual strength of samples with 12 and 14% LBM-GGBS after F-T cycles.

between 2 and 3%. During the elastic deformation stage, the stress increases rapidly with strain. After reaching the peak strain, stress drops sharply, indicating significant brittleness. This brittleness is attributed to the brittle framework formed by the hydration products of GGBS and LBM within the solidified soil, which imparts high strength³⁰. After 2 F-T cycles, as shown in Fig. 3b, the peak stress decreases significantly, and the slope of the

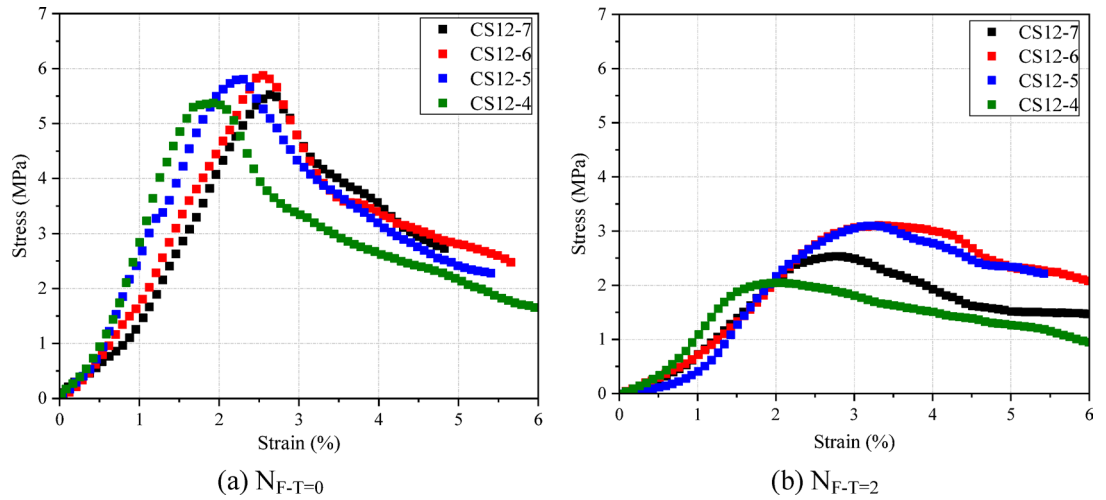


Fig. 3. Stress-strain curves of samples with 12% LBM-GGBS after 0~2 F-T cycles.

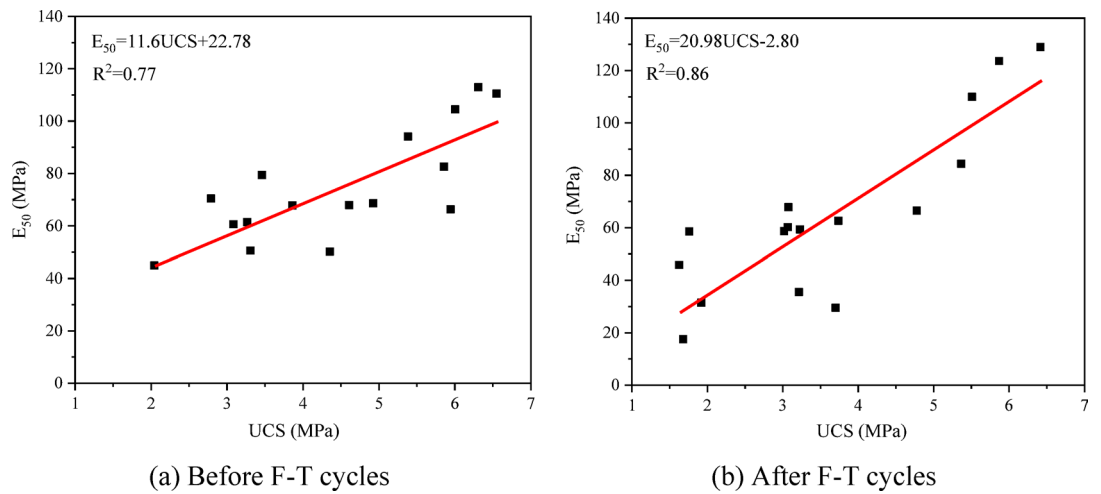


Fig. 4. Relationship between strength and deformation modules before (a) and after (b) F-T cycles.

elastic deformation stage becomes less steep. The sharp peak associated with q_u becomes less pronounced, the strain softening effect weakens, and the ductility of the solidified soil increases.

To investigate the variation in the deformation resistance of the solidified saline soil before and after F-T cycles, the deformation modulus E_{50} was introduced for analysis. This modulus is the secant modulus corresponding to the point on the stress-strain curve where the strain is half that of the failure strain. Figure 4a and b illustrate the linear relationship between the UCS and the deformation modulus before and after F-T cycles. Before F-T cycles, the relationship is expressed as $E_{50} = 11.6UCS + 22.78$, which changes to $E_{50} = 20.98UCS - 2.08$ after the F-T cycles. The increased slope of the linear fit after F-T cycles indicates that for a given change in q_u , the increase in the deformation modulus is greater, suggesting that the ability of the solidified soil to resist deformation is reduced after undergoing the F-T cycles.

Effect of F-T cycles on permeability coefficient

Permeability coefficient tests were performed on series CS8 and CS12 to evaluate the effect of LBM-GGBS content on the permeability coefficient after 0 and 10 F-T cycles, as shown in Fig. 5. Both series CS8 and CS12 demonstrate a trend of decreasing permeability coefficients with an increase in both the LBM-GGBS content and GGBS/LBM ratio. After 10 F-T cycles, the permeability coefficients for CS12 (-4, -5, -6, -7) increase from 2.48×10^{-7} , 2.22×10^{-7} , 1.78×10^{-7} , and 5.23×10^{-8} cm/s before F-T to 1.23×10^{-6} , 8.67×10^{-7} , 5.56×10^{-7} , and 4.33×10^{-7} cm/s, respectively, with changes remaining within one order of magnitude. This stability is attributed to the fact that, although the F-T process partially damages the structure of the solidified soil, the hydration products formed during the process exhibit good resistance to F-T cycles, resulting in relatively stable permeability coefficients (as detailed in Sect. 3.5). In comparison, CS8 shows significantly higher permeability coefficients after F-T cycles than CS12. This is because higher LBM-GGBS content leads to the formation of

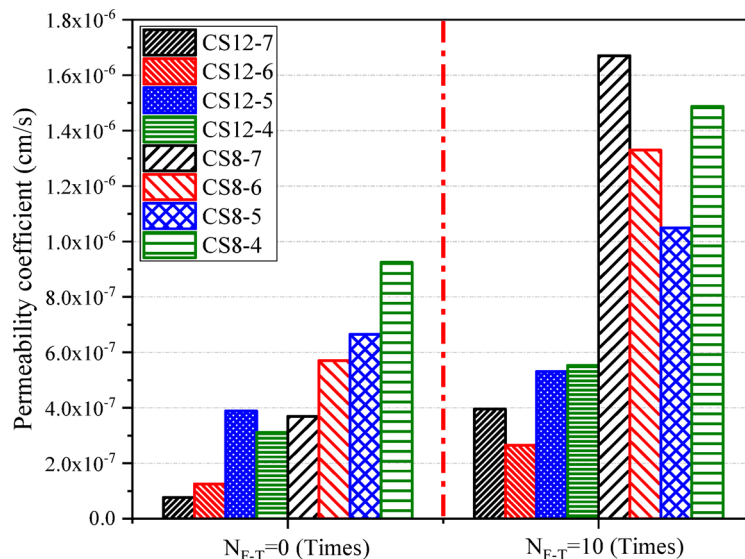


Fig. 5. Permeability coefficient of series CS8 and CS12 after 0 and 10 F-T cycles.

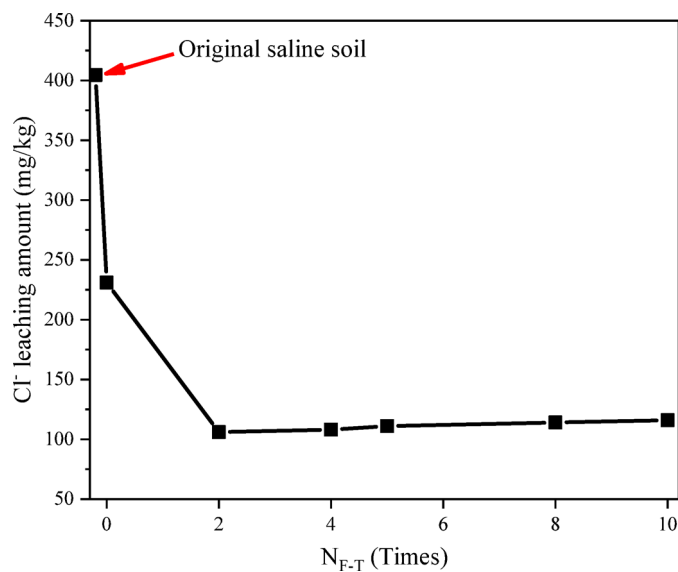


Fig. 6. Cl⁻ leaching of CS12-7 after 0, 2, and 10 F-T cycles.

more hydration products and a denser structure, thereby mitigating the impact of F-T cycles on the permeability performance of the solidified soil.

Effect of F-T cycles on Cl⁻ leaching

Figure 6 illustrates the Cl⁻ leaching of CS12-7 after 0, 2, and 10 F-T cycles. Initially, the Cl⁻ leaching from the saline soil before solidification was 404.1 mg/kg, which decreased to 230.8 mg/kg (a reduction of 42.9%) after 28 days of curing. As the number of F-T cycles increases, Cl⁻ leaching initially decreased and then stabilized, indicating that the LBM-GGBS effectively solidifies Cl⁻. More importantly, further repeated F-T cycles did not induce no obvious leaching of more Cl⁻.

Pore structure

Figure 7 illustrates the pore structure characteristics of CS12-7. As shown in Fig. 7a, the pore volume of solidified saline soil is primarily concentrated in the range of 0.1 to 1000 μm. It is noteworthy that the cumulative pore volume curves maintained high consistency across the test groups. This stability is attributed to the formation of a dense reticulate structure by the hydration products of the LBM-GGBS system. The strong cementing bonds provided sufficient resistance against internal stresses, thereby preventing the significant alteration of the pore geometry or the propagation of micro-cracks. According to Shear³¹, soil pores can be classified into

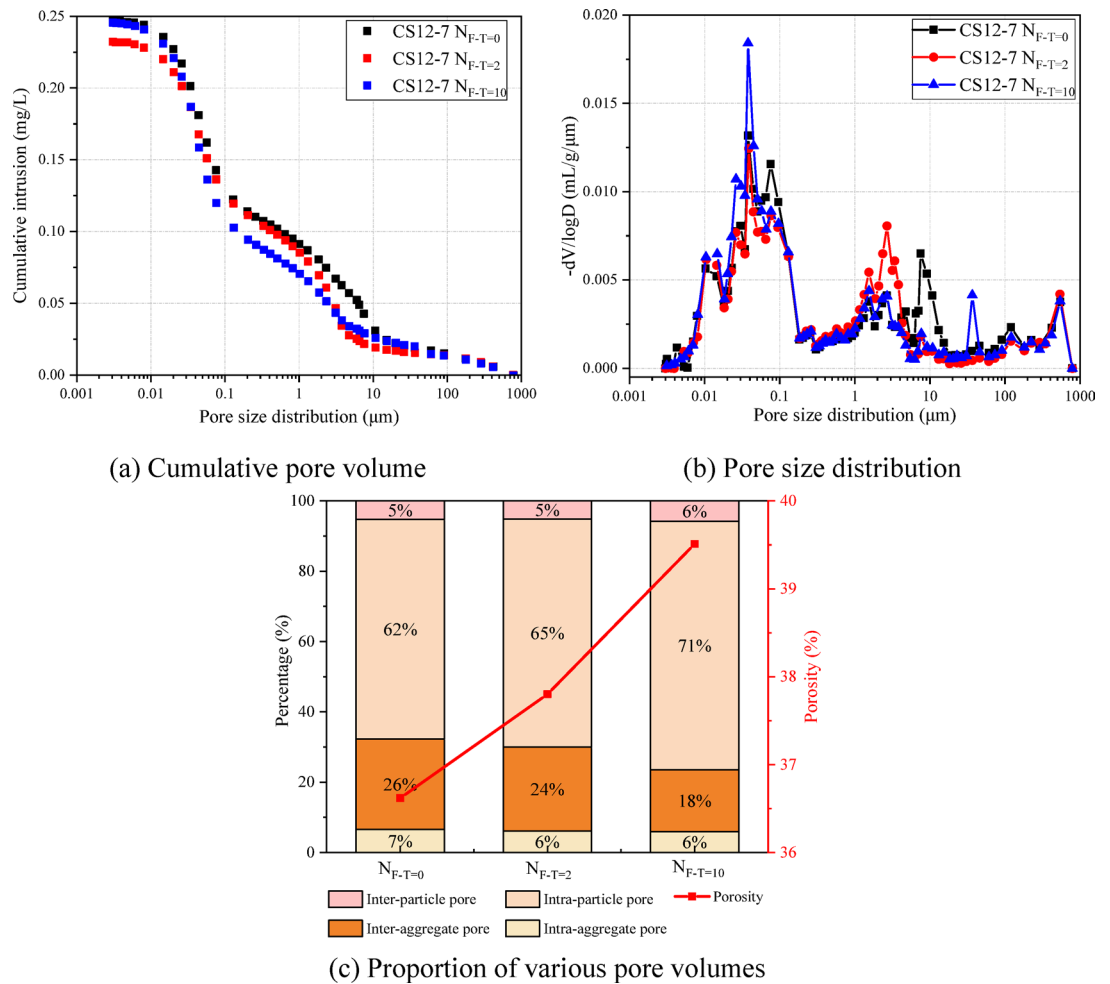


Fig. 7. Pore structure and distribution of CS12-7 after 0, 2, and 10 F-T cycles.

four categories based on their size: intra-particle pores (diameter < 0.014 μm), inter-particle pores (diameter between 0.014 and 1.800 μm), intra-aggregate pores (diameter between 1.800 and 70 μm), and inter-aggregate pores (diameter between 70 and 4000 μm). Figure 7b shows that most pores within the solidified soil fall in the diameter range of 0.01 to 0.1 μm , corresponding to intra- and inter-particle pores. After 2 F-T cycles, an obvious peak centered at 40 μm increase significantly after 10 F-T cycles. Based on the porosity and proportion of each type of pore (Fig. 7c), it is evident that the total porosity of samples gradually increases from 36.62 to 39.51% as the number of F-T cycles increases. However, a similar pore structure is observed for samples subjected to 0 and 2 F-T cycles, while the volume of inter-particle and intra-aggregate pores changes significantly from 62% to 26% to 71% and 18%, respectively.

Microstructure

Figure 8 illustrates the microstructures of the LBM-GGBS solidified saline soil after different F-T cycles. As can be seen from Fig. 8a, before any F-T cycles, the solidified soil displays a dense structure with a smooth surface, and microcracks are present between the particles. The soil particles are closely bonded to the hydration products through point-to-face and face-to-face interactions. As the number of F-T cycles increases, the small soil particles transform into larger aggregates with a flocculent surface (Fig. 8d and f). The microcracks between particles gradually disappear and instead form small pores. This transformation occurs because the primary hydration product of Mg^{2+} in the LBM-GGBS stabilized soil is hydrotalcite (Ht), which features a rose-like layered network structure with a large specific surface area³². This structure not only fills microcracks within the soil but also creates a few larger pores between and within the particles. Despite these changes, the needle-like, lamellar, and flocculent hydration products remain clearly visible and maintain a dense network structure. This suggests that the hydration products are minimally affected by the F-T cycles, allowing the solidified soil to retain a good strength even after these cycles.

To identify the specific phases resulting from the hydration reaction, EDS analysis was conducted in conjunction with SEM. The analysis reveals a high silicon (Si) content in the needle-like and lamellar phases (points 1 and 2). This is likely because the diameter of the detection point is larger than the size of the chloride

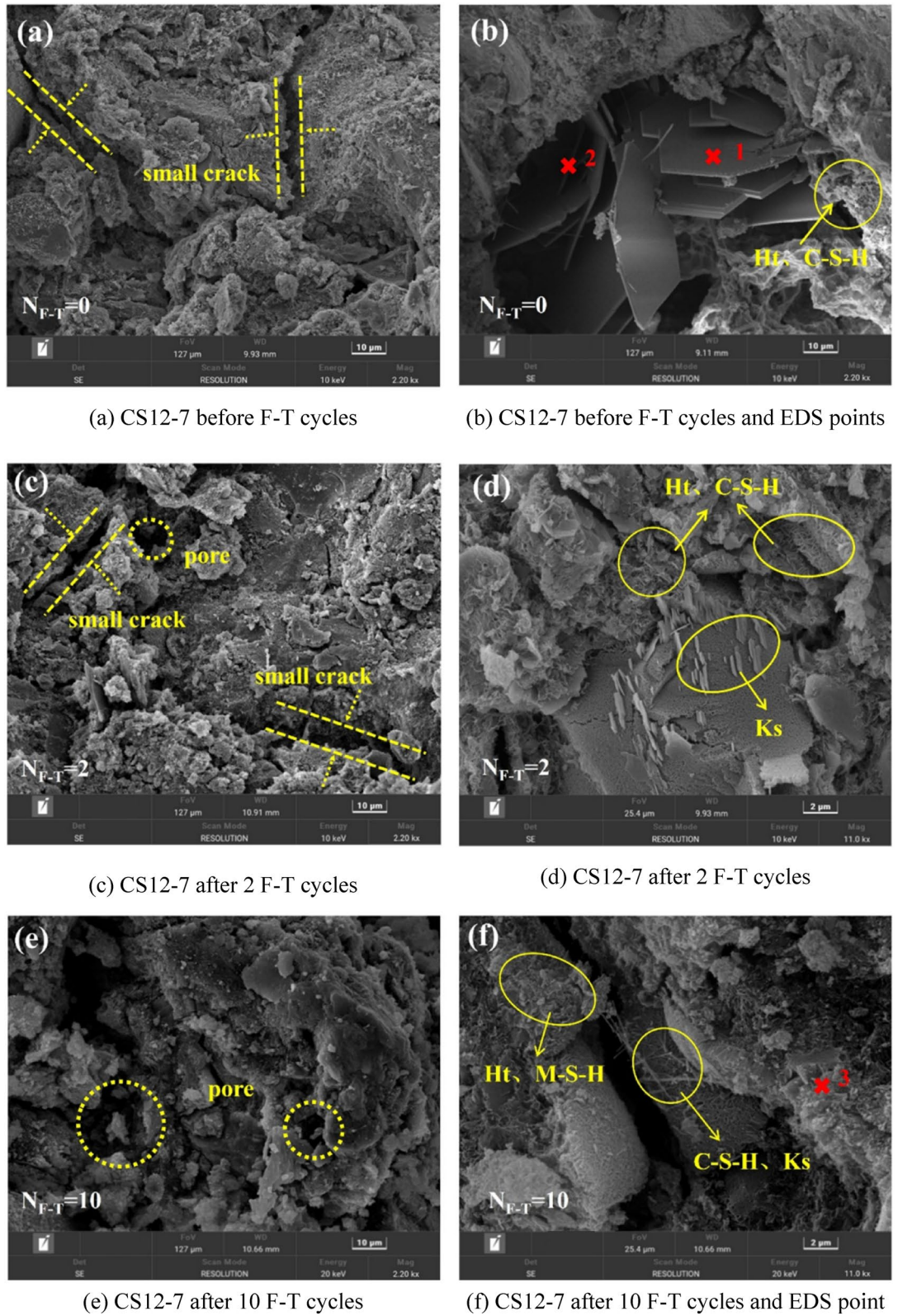


Fig. 8. SEM images of CS12-7 after 0, 2 and 10 F-T cycles.

(Cl⁻) containing compounds, leading to the inclusion of C-S-H gels in the detection points. To minimize the influence of C-S-H gels, it is assumed that the calcium-to-silicon (Ca/Si) ratio of C-S-H is 1, and all Si initially forms C-S-H gels. After accounting for the Si and Ca required for C-S-H gels, the average atomic ratios of the remaining elements of Ca: Al: S: Cl in points 1 and 2 are 7.87: 3.94: 1: 1.98, as shown in Table 5, which closely

	Elements	O	Na	Mg	Al	Si	S	Cl	Ca
Spot 1	Total element content(%)	37.14	0.46	1.41	12.03	3.85	1.96	5.64	37.51
	Content of Ca & Si in C-S-H gel(%)	-	-	-	-	3.85	-	-	5.49
	Content of remaining elements(%)	37.14	0.46	1.41	12.03	0	1.96	5.64	32.02
	Atomic ratio of remaining elements	-	-	-	7.17	-	1	2.6	13.05
Spot 2	Total element content(%)	47.56	1.05	1.45	7.27	6.68	4.36	1.59	30.3
	Content of Ca & Si in C-S-H gel(%)					6.68			9.54
	Content of remaining elements(%)	47.56	1.05	1.45	7.27	0	4.36	1.59	20.76
	Atomic ratio of remaining elements	-	-	-	1.99	-	1	0.33	3.82

Table 5. EDS results of CS12-7.

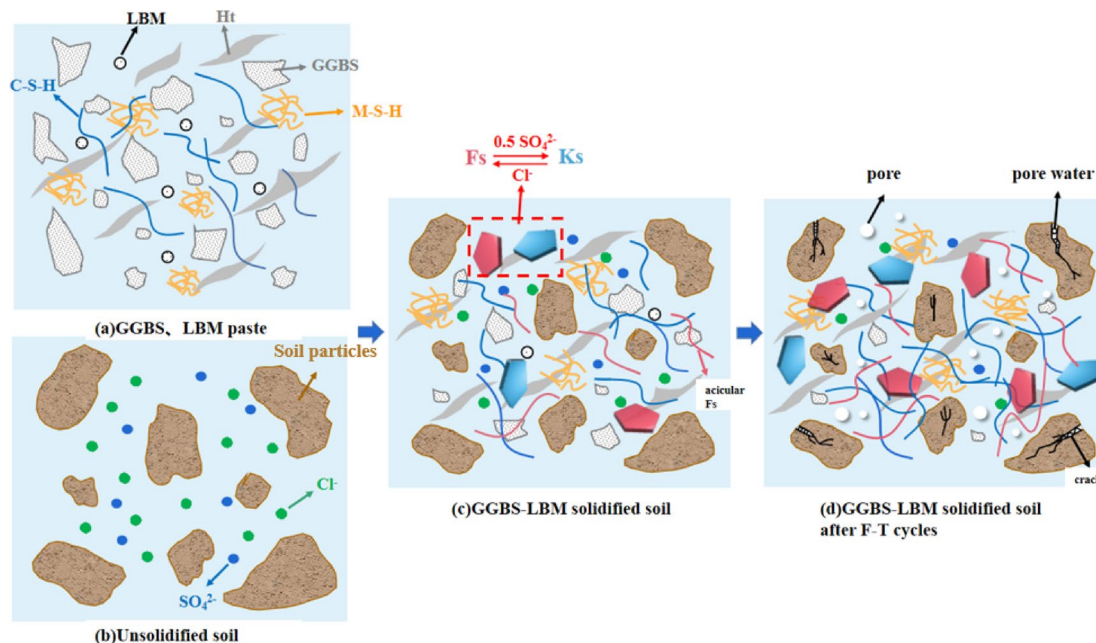


Fig. 9. Reaction mechanisms of LBM-GGBS with saline soil.

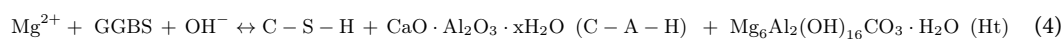
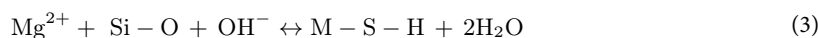
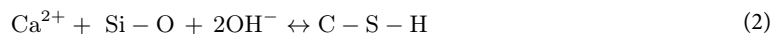
matches the composition of $3\text{CaO}\cdot\text{Al}_2\text{O}_3\cdot(0.5\text{CaCl}_2\cdot0.5\text{CaSO}_4)\cdot12\text{H}_2\text{O}$, known as Kuzel salt (Ks). In an alkaline environment, the chloride salts in saline soil can chemically interact with silicate and aluminate in GGBS to form $3\text{CaO}\cdot\text{Al}_2\text{O}_3\cdot\text{CaCl}_2\cdot10\text{H}_2\text{O}$, also known as Friedel's Salt (Fs)³³. However, the presence of SO_4^{2-} in saline soil may cause partial substitution of Cl^- , leading to the formation of multiple complex compounds. Based on the EDS results, it can be concluded that the compounds formed at points 1 and 2 are Ks.

Existing research has shown that the reaction between MgO and GGBS can produce compounds such as calcium silicate hydrate (C-S-H), magnesium silicate hydrate (M-S-H) gel, and Ht³⁴. In the LBM-GGBS solidified saline soil, Mg^{2+} primarily contributes to the formation of M-S-H and hydrotalcite (Ht). In Fig. 8f, point 3 shows a Mg to Al atomic ratio of 1.85, whereas the typical Mg to Al atomic ratio in Ht compounds is 3. Additionally, the Mg to Si atomic ratio at this point is 2, compared with the standard ratio of 1.5 in M-S-H³⁵. Therefore, it is concluded that point 3 represents a mixture of M-S-H and Ht. Figure 8b,d,e illustrate the formation of a substantial amount of lamellar and needle-like Ks, along with flocculent hydration products of C-S-H and M-S-H. The rose-like layered Ht and the flocculent fibrous C-S-H and M-S-H gels are interwoven with each other, consistent with the findings of Bo³⁵ and Jin et al.³⁶.

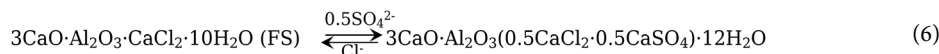
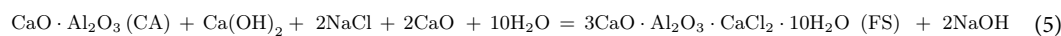
Discussion

The mechanisms for solidifying saline soil using LBM-GGBS involve several key steps: (1) the dissolution of LBM and saline soil in water releases OH^- , Na^+ , K^+ , Mg^{2+} and Ca^{2+} ions, creating a favorable alkaline environment for the activation of GGBS^{34,37}; (2) the breaking of Al-O and Si-O bonds in GGBS due to the erosion of OH^- ; (3) the combination of Ca^{2+} and Mg^{2+} ions with Al-O and Si-O bonds to form compounds such as C-S-H, M-S-H, and Ht, as illustrated in Fig. 9a. The primary hydration reaction equations are as follows:





Additionally, GGBS can be chemically activated by the NaCl present in saline soil. This occurs through the reaction between Cl^- ions and calcium aluminate in GGBS, resulting in the formation of Fs, as shown in Eq. (5). However, the presence of SO_4^{2-} in the saline soil causes mutual substitution between Cl^- and SO_4^{2-} , leading to a transition of hydration products from Fs to Ks, as depicted in Eq. (6).



For natural saline soil, the repeated crystallization and dissolution of salts during F-T cycles can cause structural damage³⁸. Similarly, when solidified soil freezes, the pore water between soil particles and the remaining pore salt solution freeze into ice, causing volume expansion and exerting stress on the surrounding soil particles. This results in F-T cracks and structural damage, which will not completely disappear after the ice melts³⁸. Consequently, the strength of the solidified soil decreases after F-T cycles, the porosity increases, and the permeability coefficient rises. The increase in the LBM-GGBS content could effectively enhance the overall production of various reaction products, resulting in a denser structure and higher UCS of the solidified soil. This significantly improves its resistance to F-T cycles. The optimal ratio can be achieved at 12% LBM-GGBS content and the GGBS/LBM of 7. Under these conditions, the solidified soil maintains a strength of 3 MPa even after 10 F-T cycles. Furthermore, when the LBM-GGBS content exceeds 10%, the strength remains above 1.3 MPa after multiple F-T cycles. However, adding excessive GGBS reduces alkalinity within the system, leading to the accumulation of unreacted GGBS. This may adversely affect the strength of the solidified soil. Comparing the solidification effects of curing agents reported in the literature for saline soils, the combination of LBM and GGBS proves to be the most effective. This performance surpasses the UCS of saline soils solidified with lime (584 kPa)³⁹, cement (475 kPa)⁴⁰, and a combination of lime and fly ash (1130.25 kPa)⁴¹.

Figure 8d and f illustrate that even after undergoing F-T cycles, the LBM-GGBS stabilized soil retains prominent needle-like and flaky hydration products. These needle-like structures (Ks), formed prior to the F-T process, demonstrate excellent F-T resistance. As curing progresses, the quantity of hydration products such as M-S-H and C-S-H increases, creating a flocculent fibrous network interwoven with rose-like layered Ht, which provides robust cementation (Fig. 9d). This structural integrity ensures that the samples remain largely undamaged after F-T cycles, with only a slight increase in small pore sizes within the aggregates. Additionally, as the number of F-T cycles increases, there is a noticeable decrease in Cl^- leaching from the stabilized soil, suggesting that Cl^- actively participates in the hydration reaction throughout the F-T process. Measurements of the height and diameter of the samples after F-T reveal no volume expansion, indicating that while repeated F-T cycles may inflict some microstructural damage, the superior F-T resistance of the Ks hydration products significantly mitigates such damage. Unlike the detrimental effects of Cl^- in the un-stabilized soil during F-T cycles, within the LBM-GGBS system, Cl^- instead contributes positively to the stabilized soil's performance.

Conclusions

This study elucidates the deterioration mechanism and stabilization efficacy of LBM-GGBS solidified saline soil under freeze-thaw (F-T) cycles. Based on the mechanical and microstructural evaluations, the key findings can be summarized as follows:

- (1) The samples designated as CS12-7 (12% binder dosage, GGBS/LBM ratio of 7) demonstrated superior durability. Even after 10 F-T cycles, it retained a residual strength of 3 MPa, which is four times greater than the standard requirement for highway pavement upper base layers (JTJ034-2000). This confirms that the CS12-7 mix offers an optimal balance of cost-effectiveness and mechanical performance.
- (2) The solidified soil exhibited typical brittle failure characteristics, characterized by strain-softening behavior. The soil subjected to F-T cycles altered this behavior; specifically, the peak stress decreased, the elastic modulus degraded, and the failure strain increased, reflecting an improvement in ductility beyond the peak stress.
- (3) The incorporation of LBM-GGBS significantly mitigated chloride leaching, achieving a 43% reduction (from 404.1 to 230.8 mg/kg) compared to the original saline soil. Crucially, the leaching concentration continued to decline with ongoing F-T cycles, indicating that the chemical binding capacity of the hydration products outweighs the physical leaching effects caused by structural damage.
- (4) The LBM-GGBS solidified saline soil exhibits a dense structure, with C-S-H, M-S-H and hydrotalcite (Ht) as the primary hydration products. The Cl^- and SO_4^{2-} in the soil could react with GGBS to form hydration products Friedel's Salt (Fs) and Kuzel's Salt (Ks). These hydration products exhibit excellent resistance to degradation during F-T cycles, ensuring that the solidified soil retains excellent strength and Cl^- stabilization after multiple cycles.

Data availability

All data supporting the findings of this study are available from the author upon request from the corresponding author.

Received: 21 December 2025; Accepted: 24 March 2026

Published online: 27 March 2026

References

- Li, H. et al. Characterization and mechanism study of sulfate saline soil solidification in seasonal frozen regions using ternary solid waste-cement synergy. *Constr. Build. Mater.* **427**, 136263 (2024).
- Katarzyna Negacz, A., de Vos, P. Vellinga Saline soils worldwide: Identifying the most promising areas for saline agriculture. *J. Arid Environ.* **203** 104775. (2022).
- Zhu, B. & Yang, X. The origin and distribution of soluble salts in the sand seas of northern China. *Geomorphology* **123** (3), 232–242 (2010).
- Wang, L., Zhao, Z. Y., Zhang, K. & Tian, C. Y. Reclamation and Utilization of Saline Soils in Arid Northwestern China: A Promising Halophyte Drip-Irrigation System. *Environ. Sci. Technol.* **47** (11), 5518–5519 (2013).
- Wang, S. et al. Insights into the Microbial Diversity in Saline-Alkaline Soils of China, in: (eds Egamberdieva, D., Birkeland, N. K., Li, W. J. & Panosyan, H.) *Microbial Communities and their Interactions in the Extreme Environment*, Springer Singapore, Singapore, 17–41. (2021).
- Xueying Zhao, A., Shen, Y., Guo, P., Li, Z. & Lv Pavement mechanic response of sulfate saline soil subgrade section based on fluid-structure interaction model. *Int. J. Pavement Res. Technol.* **10** (6), 497–506 (2017).
- Zhang, Y. et al. Impact of isothermal layering on the stability of saline soil subgrade in cold regions. *Geofluids* **2022** (1), 3141964. (2022).
- Samimifar, R. Z. M. M. & Kamalzare, M. Improvement of shear strength characteristics of saline soil using cement and polymer. *Int. J. Geotech. Eng.* **5** (3), 307–314 (2011).
- Pitthaya Jamsawang, H., Poorahong, N., Yoobanpot, S., Songpiriyakij, P. & Jongpradist Improvement of soft clay with cement and bagasse ash waste. *Constr. Build. Mater.* **154**, 61–71 (2017).
- Nabilla Mohamad, K., Muthusamy, R., Embong, A. & Kusbiantoro Mohd Hanafi Hashim. Environmental impact of cement production and solutions: A review. *Mater. Today Proc.* **48** 741–746. (2022).
- Zhen He, R., Cai, E., Chen, S. & Tang The investigation of early hydration and pore structure for limestone powder wastes blended cement pastes. *Constr. Build. Mater.* **229**, 116923 (2019).
- Adeleke, B. O., Kinuthia, J. M. & Oti, J. E. Impacts of MgO waste:GGBS formulations on the performance of a stabilised natural high sulphate bearing soil. *Constr. Build. Mater.* **315**, 125745 (2022).
- Jiang, N. J., Du, Y. J. & Liu, K. Durability of lightweight alkali-activated ground granulated blast furnace slag (GGBS) stabilized clayey soils subjected to sulfate attack. *Appl. Clay Sci.* **161**, 70–75 (2018).
- Yaolin Yi, L., Gu, S. & Liu Microstructural and mechanical properties of marine soft clay stabilized by lime-activated ground granulated blastfurnace slag. *Appl. Clay Sci.* **103**, 71–76 (2015).
- Chenbing Liu, H., Ji, J., Liu, W., He, C. & Gao Experimental study on slag composite cementitious material for solidifying coastal saline soil. *J. Building Mater.* **18** (01), 82–87 (2015).
- Fei Jin, K., Gu, A. & Al-Tabbaa Strength and hydration properties of reactive MgO-activated ground granulated blastfurnace slag paste. *Cem. Concr. Compos.* **57**, 8–16 (2015).
- Karimi, H. & Brouwers, H. J. H. Accelerated thermal history analysis of light-burnt magnesium oxide by surface properties. *Results Mater.* **17**, 100368 (2023).
- Yu, H., Yi, Y. & Unluer, C. Heat of hydration, bleeding, viscosity, setting of Ca(OH)₂-GGBS and MgO-GGBS grouts. *Constr. Build. Mater.* **270**, 121839 (2021).
- Yaolin Yi, M., Liska, A. & Al-Tabbaa Properties and microstructure of GGBS-MgO pastes. *Adv. Cem. Res.* **26** (2), 114–122 (2014).
- Yaolin Yi, M., Liska, A. & Al-Tabbaa. Initial investigation into the use of GGBS-MgO in soil stabilisation, grouting and deep mixing. **2012** 444–453. (2012).
- Dongxing Wang, D. et al. Freeze-thaw cycle and temperature effect of reactive MgO-fly ash stabilized Pb-contaminated soils (In Chinese). *Eng. J. Wuhan Univ.* **54** (7), 609–617 (2021).
- Guanghua Cai, S. et al. Mechanical performances and microstructural characteristics of reactive MgO-carbonated silt subjected to freezing-thawing cycles. *J. Rock Mech. Geotech. Eng.* **13** (4), 875–884 (2021).
- GB/T50123. Standard for geotechnical testing method, Ministry of Housing and Urban-Rural Development of the People's Republic of China & State Administration for Market Regulation, Beijing, (2019).
- GB50021-2001. *Code for Investigation of Geotechnical Engineering*, Ministry of Construction & General Administration of Quality Supervision (Inspection and Quarantine of the People's Republic of China, 2002).
- Guanghua Cai, S. & Liu Compaction and mechanical characteristics and stabilization mechanism of carbonated reactive MgO-stabilized silt. *KSCE J. Civ. Eng.* **21** (7), 2641–2654 (2017).
- Wang, D., Wang, H., Zou, W. & Xu, X. Study of durability of dredged sludge solidified with reactive MgO-fly ash. *Rock. Soil. Mech.* **40** (12), 4675–4684 (2019).
- ASTM D5084. *Standard Test Method for Measurement of Hydraulic Conductivity of Saturated Porous Materials Using a Flexible Wall Permeameter* (American Society for Testing and Materials, 1997).
- Manikanta Devarangadi, M., Uma & Shankar Effect on engineering properties of ground granulated blast furnace slag admixed with laterite soil, cement and bentonite mixtures as a liner in landfill. *J. Clean. Prod.* **329**, 129757 (2021).
- JTJ034, Highway Pavement Subgrade Construction Technical Specifications. Ministry of Communications of the People's Republic of China, (2000).
- Qiang Fu, Z., Wang, Z., Zhou, D., Niu, Y. & Wang Feasible brittleness evaluation method and suggestion for brittleness reduction of cementitious materials based on stress-strain curve. *Archives Civil Mech. Eng.* **22** (4), 209 (2022).
- Dixie, L., Shear, H. W., Olsen, K. R. & Nelson *Effects of Desiccation on the Hydraulic Conductivity versus Void Ratio Relationship for a Natural Clay* (National Academy, 1992).
- Cao, C. Y., Nie, M. H., Chen, S. L., Wang, W. L. L. M. & Zhao, S. Xin Wan, Zhi-Guo Song, The calcined Mg-Al hydrotalcite for copper adsorption and passivation of copper-contaminated soil. *Process Saf. Environ. Prot.* **197**, 107015 (2025).
- Cheng, Y., Li, Z., Huang, X. & Bai, X. Effect of Friedel's salt on strength enhancement of stabilized chloride saline soil. *J. Cent. South. Univ.* **24** (4), 937–946 (2017).
- Zheng, J., Sun, X., Guo, L., Zhang, S. & Chen, J. Strength and hydration products of cemented paste backfill from sulphide-rich tailings using reactive MgO-activated slag as a binder. *Constr. Build. Mater.* **203**, 111–119 (2019).
- Yulin & Bo The strength, leaching and microscopic mechanism of ground granulated blast furnace slag and magnesium oxides stabilized lead-contaminated soils (In Chinese), Southeast University, Nanjing, (2015).
- Fei Jin, K., Gu, A., Abdollahzadeh, A. & Al-Tabbaa Effects of Different Reactive MgOs on the Hydration of MgO-Activated GGBS Paste. *J. Mater. Civ. Eng.* **27** (7), B4014001 (2015).
- Zhang, Y., Ong, Y. J. & Yi, Y. Comparison between CaO- and MgO-activated ground granulated blast-furnace slag (GGBS) for stabilization/solidification of Zn-contaminated clay slurry. *Chemosphere* **286**, 131860 (2022).
- Lai, Y., Wu, D. & Zhang, M. Crystallization deformation of a saline soil during freezing and thawing processes. *Appl. Therm. Eng.* **120**, 463–473 (2017).

39. Zhang, W., Ma, J. & Tang, L. Experimental study on shear strength characteristics of sulfate saline soil in Ningxia region under long-term freeze-thaw cycles. *Cold Reg. Sci. Technol.* **160**, 48–57 (2019).
40. Li & Guo *Experimental Study on Resistivity and Strength Characteristics of Cement-cured Soil under Freeze-thaw Cycle* (Southwest University of Science and Technology, 2019).
41. Li, M., Yu, H. & Du, H. Mechanical properties of saline soil solidified with the mixture of lime, fly ash and modified polyvinyl alcohol under freeze-thaw cycles. *Rock. Soil. Mech.* **43** (2), 489–498 (2022).

Acknowledgements

The authors would like to acknowledge the financial support of the National Natural Science Foundation of China (Grants No. 42107185).

Author contributions

Shanyan Chen wrote the original manuscript draft. Pengfei Ren, Junyi Wang, and Yang Zhao reviewed and edited the manuscript text. Ming-Zhi Guo provided the funding support. Ziqing He and Gang Hou were responsible for the data collection. Jiang-Shan Li supervised the manuscript.

Declarations

Competing interests

The authors declare no competing interests.

Additional information

Correspondence and requests for materials should be addressed to P.R. or J.W.

Reprints and permissions information is available at www.nature.com/reprints.

Publisher's note Springer Nature remains neutral with regard to jurisdictional claims in published maps and institutional affiliations.

Open Access This article is licensed under a Creative Commons Attribution-NonCommercial-NoDerivatives 4.0 International License, which permits any non-commercial use, sharing, distribution and reproduction in any medium or format, as long as you give appropriate credit to the original author(s) and the source, provide a link to the Creative Commons licence, and indicate if you modified the licensed material. You do not have permission under this licence to share adapted material derived from this article or parts of it. The images or other third party material in this article are included in the article's Creative Commons licence, unless indicated otherwise in a credit line to the material. If material is not included in the article's Creative Commons licence and your intended use is not permitted by statutory regulation or exceeds the permitted use, you will need to obtain permission directly from the copyright holder. To view a copy of this licence, visit <http://creativecommons.org/licenses/by-nc-nd/4.0/>.

© The Author(s) 2026